SOURCE DATA · TRANSPARENT PROCESS · OPEN ACCESS

THE EMBO JOURNAL

Antitumor T-cell function requires CPEB4-mediated adaptation to chronic endoplasmic reticulum stress

Marcos Fernández-Alfara[1] [ID], Annarita Sibilio[1] [ID], Judit Martin[1] [ID], Elsa Tusquets Uxó[1] [ID], Marina Malumbres[1] [ID], Victor Alcalde[1], Verónica Chanes[1], Adrià Cañellas-Socias[1] [ID], Sergio Palomo-Ponce[1] [ID], Eduard Batlle[1,2] & Raúl Méndez[1,2,*] [ID]

Abstract

Tumor growth is influenced by a complex network of interactions between multiple cell types in the tumor microenvironment (TME). These constrained conditions trigger the endoplasmic reticulum (ER) stress response, which extensively reprograms mRNA translation. When uncontrolled over time, chronic ER stress impairs the antitumor effector function of CD8 T lymphocytes. How cells promote adaptation to chronic stress in the TME without the detrimental effects of the terminal unfolded protein response (UPR) is unknown. Here, we find that, in effector CD8 T lymphocytes, RNA-binding protein CPEB4 constitutes a new branch of the UPR that allows cells to adapt to sustained ER stress, yet remains decoupled from the terminal UPR. ER stress, induced during CD8 T-cell activation and effector function, triggers CPEB4 expression. CPEB4 then mediates chronic stress adaptation to maintain cellular fitness, allowing effector molecule production and cytotoxic activity. Accordingly, this branch of the UPR is required for the antitumor effector function of T lymphocytes, and its disruption in these cells exacerbates tumor growth.

Introduction

Tumor growth depends not only on the intrinsic properties of the cancerous cells but also on its communication with the tumor microenvironment (TME). The TME is a heterogeneous mix of active endothelial cells, fibroblasts, and immune cells that interact through secreted and membrane proteins (Quail & Joyce, 2013). The high metabolic activity of cancerous and non-cancerous cells generates a limiting hypoxic, acidic, and nutrient-deprived TME that can impair cellular function (Chang *et al*, 2015; Leone *et al*, 2019; Elia & Haigis, 2021). These harsh conditions, coupled with the high demand for protein modification and folding to sustain secretory activity, lead to high levels of chronic stress that activate the unfolded protein response (UPR) in the cells of the TME. ER stress responses need duration-dependent adaptation programs, and the UPR, although initially beneficial for the cell, activates a terminal response that compromises cellular fitness and function. The early response involves translational repression, which is directly mediated by eIF2α phosphorylation, while the late response requires transcriptional regulation. This canonical UPR program is directed toward stress resolution or, if unresolved, cell death outcomes. Accordingly, for T lymphocytes subjected to chronic stress in the TME, canonical UPRs are detrimental to their antitumoral effector responses (Song *et al*, 2018; Cao *et al*, 2019; Ma *et al*, 2019). Chronic ER stress requires transcript-specific regulation while global translation is sustained, and it also has to be decoupled from cell death. The mechanisms that uncouple the adaptive and terminal UPR in chronic stress situations are largely unknown, and the translational regulation program is much less defined, eIF3 and CPEB4 being potential regulatory candidates (Guan *et al*, 2017; Maillo *et al*, 2017).

The regulation of translation is pivotal for tumor development, as it controls not only the intrinsic properties of cancer cells (such as proliferation and stemness) but also bidirectional communication between these cells and the TME (Robichaud *et al*, 2018; Xu & Ruggero, 2020; Chen & Cubillos-Ruiz, 2021; Fabbri *et al*, 2021). The cytoplasmic polyadenylation element-binding (CPEB) family of RNA-binding proteins regulates mRNA localization and translation by recognizing a cis-acting element, namely the cytoplasmic polyadenylation element (CPE), present in the 3′ UTR of target mRNAs. In turn, CPEBs regulate the translation and stability of mRNAs through changes in the length of their poly(A) tails (Fernandez-Miranda & Mendez, 2012; Ivshina *et al*, 2014). The stress-regulated member of the CPEB family, CPEB4, is required in a cell-autonomous manner for the survival and proliferation of tumor cells (Ortiz-Zapater *et al*, 2011; Perez-Guijarro *et al*, 2016; Tsai *et al*, 2016; Maillo *et al*, 2017; Villanueva *et al*, 2017; Cao *et al*, 2018).

1 Institute for Research in Biomedicine (IRB Barcelona), The Barcelona Institute of Science and Technology, Barcelona, Spain
2 Institució Catalana de Recerca i Estudis Avançats (ICREA), Barcelona, Spain
*Corresponding author. Tel: +34 649483634 ; E-mail: raul.mendez@irbbarcelona.org

However, its role in rewiring translation in other cell types present in the TME in response to stress is still unknown.

Here, we address whether translational regulation by CPEB4 in non-cancerous cells of the TME affects tumor development. We found that, in T lymphocytes, CPEB4 is a novel branch of the adaptive UPR that is decoupled from terminal UPR. CPEB4-mediated adaptation to chronic ER stress sustains T-cell effector function and, accordingly, CPEB4 is required in T lymphocytes for efficient antitumor responses. We conclude that CPEB4 mediates antitumor immunity through its action as a novel adaptive branch of the UPR in T cells.

Results

Depletion of CPEB4 in T lymphocytes impairs T cell-mediated antitumor immunity

To study whether CPEB4 function in non-cancerous cells of the TME influences tumor growth, we subcutaneously allografted CPEB4-expressing B16F10 melanoma cells into syngeneic mice that were wild-type (WT, $Cpeb4^{+/+}$) or knock-out for CPEB4 (KO, $Cpeb4^{-/-}$) (Fig 1A). Interestingly, tumor growth was enhanced in KO hosts as compared to WT mice (Fig 1B). Comparative flow cytometry analysis of tumors (Fig EV1A) showed that the TMEs from KO animals were less infiltrated with cytotoxic CD8 T lymphocytes than those from WT mice (Fig 1C). In contrast, no differences were observed in the infiltration of total CD45 immune cells, CD4 T cells, CD11b myeloid cells, or CD11bF4/80 macrophages (Fig EV1B–E) by flow cytometry, or fibroblasts and endothelial cells, as detected by immunostaining (Fig EV1F and G). We next analyzed melanoma metastatic burden by tail vein injection of B10F10 cells expressing luciferase into WT and KO mice, followed by measurements of luciferase signal in the lung up to 14 days post-injection (DPI). Regarding primary tumors, metastatic burden was also increased in KO hosts (Fig EV1H). The increased luciferase signal originated from larger metastatic foci, rather than from an increased number of foci

(Figs 1D and E, and EV1I), suggesting that a lack of CPEB4 in the TME cells affected metastasis growth rather than metastatic homing. Moreover, CD3 immunostaining showed reduced infiltration of T lymphocytes in whole lungs from KO animals (Fig EV1J). Taken together, these results indicate that CPEB4 depletion from the cells in the TME favors tumor growth and suggest that this effect is mediated through T cells.

To address whether the antitumor effect of CPEB4 in the TME was T lymphocyte specific, we used a CD4-Cre mouse line to specifically deplete CPEB4 from CD4 and CD8 T cells (CPEB4 T cell KO, herein TKO). As expected, CPEB4 protein levels were depleted in CPEB4-TKO thymocytes (Fig EV2A). Of note, CPEB4-TKO mice had no alterations in thymus weight or cellularity, as compared with (Cre^+) control mice (Fig EV2B and C). Additionally, CPEB4-TKO mice showed normal T=cell development in the thymus (Fig EV2D–K) and had normal numbers and frequencies of T cells in blood, spleen, and lymph nodes (Fig EV2L and M). Naïve–effector–memory lymphocyte subset distributions were also unaffected in the CPEB4-TKO (Fig EV2N and O).

To test whether the T cell-mediated antitumor response required CPEB4, we subcutaneously injected B16F10OVA cells (which express the ovalbumin (OVA) antigen that potentiates immune recognition (Sancho et al, 2008)) intro Cre^+ and CPEB4-TKO hosts. Similar to the whole-body CPEB4 KO, specific T-cell depletion caused larger tumors in TKO mice as compared to Cre^+ controls (Fig 1F), with reduced survival (Fig 1G). To test whether this effect was specific only to the melanoma model, we also performed intra-spleen injection of colorectal cancer organoids expressing luciferase (Tauriello et al, 2018) and tracked luciferase activity to monitor metastatic growth (Fig 1H). Indeed, the metastatic burden also increased in the TKO mice, thereby pointing to a functional defect in T cells that supported tumor growth across models.

We next measured CD8 T-cell infiltration in B16F10OVA tumors by FACS (Figs 2I and EV3A) and immunofluorescence (Fig EV3B). CD8 infiltration was reduced in CPEB4-TKO mice, while CD4 T-cell levels were unaffected (Fig EV3C). We next analyzed T-cell functionality by measuring the production of T-cell effector molecules in

---

Figure 1. T cell-specific loss of CPEB4 impairs antitumor immunity.

A   Schematic representation of the experimental design.

B   Tumor growth of B16F10 cells injected subcutaneously into WT ($Cpeb4^{+/+}$) ($n = 8$) and CPEB4 KO ($Cpeb4^{-/-}$) mice ($n = 9$).

C   Flow cytometry analysis of CD8 T-cell infiltration in B16F10 tumors from WT or KO mice 14 days post-injection (DPI) ($n = 7$ per genotype).

D, E Lung metastasis foci number (D) and area (E) from WT ($n = 20$) or KO ($n = 21$) mice injected via tail vein with B16F10 TGL cells at 14 DPI.

F, G Tumor growth (F) and survival curves (G) of Cre^+ or TKO mice injected subcutaneously with B16F10 OVA cells ($n = 7$ per genotype). Survival time was defined as the time required for a tumor to reach a volume of 500 mm³.

H   Quantification of bioluminescence signal of liver metastasis from Cre^+ or TKO mice injected intra-spleen with colorectal cancer organoids expressing luciferase ($n = 10$ per genotype).

I   Flow cytometry analysis of CD8 T-cell infiltration in B16F10 OVA tumors from Cre^+ ($n = 16$) or TKO ($n = 11$) mice 14 DPI.

J   Representative plots (left panels) and quantification (right panels) of IFNγ- and TNFα-producing CD8 TILs of B16F10 OVA tumors from Cre^+ ($n = 10$) and TKO ($n = 12$) animals at day 14.

K   Representative plot (upper panel) and quantification (lower panel) of GZMB median fluorescent intensity (MFI) of CD8 in tumors from Cre^+ ($n = 15$) and TKO ($n = 11$) mice injected s.c. with B16F10 OVA cells. MFI values are normalized to Cre^+ mice.

L   Representative plots (left panels) and quantification (right panels) of IFNγ- and TNFα-producing CD8 splenocytes of B16F10 OVA tumor-bearing Cre^+ ($n = 7$) and TKO ($n = 7$) animals.

Data information: Data are represented as mean ± s.d., except in (B, H) where points and lines represent individual mice, trend lines (bold) show (B) a spline curve, and (H) a LOESS model with 95% confidence interval (gray band). In (D, E), data are shown as a box (the median is middle band) with whiskers (min and max). Statistical analysis was performed by two-way ANOVA with Sidak correction (B, F), Mann–Whitney test (C, D, E, I–L), linear model with random effects (H), and Mantel–Cox test (G). Exact P-values are indicated in the graphs; ns = not significant. The data are representative of two to four independent experiments (B, C, F–H) or pooled from two independent experiments (D, E, I–L).
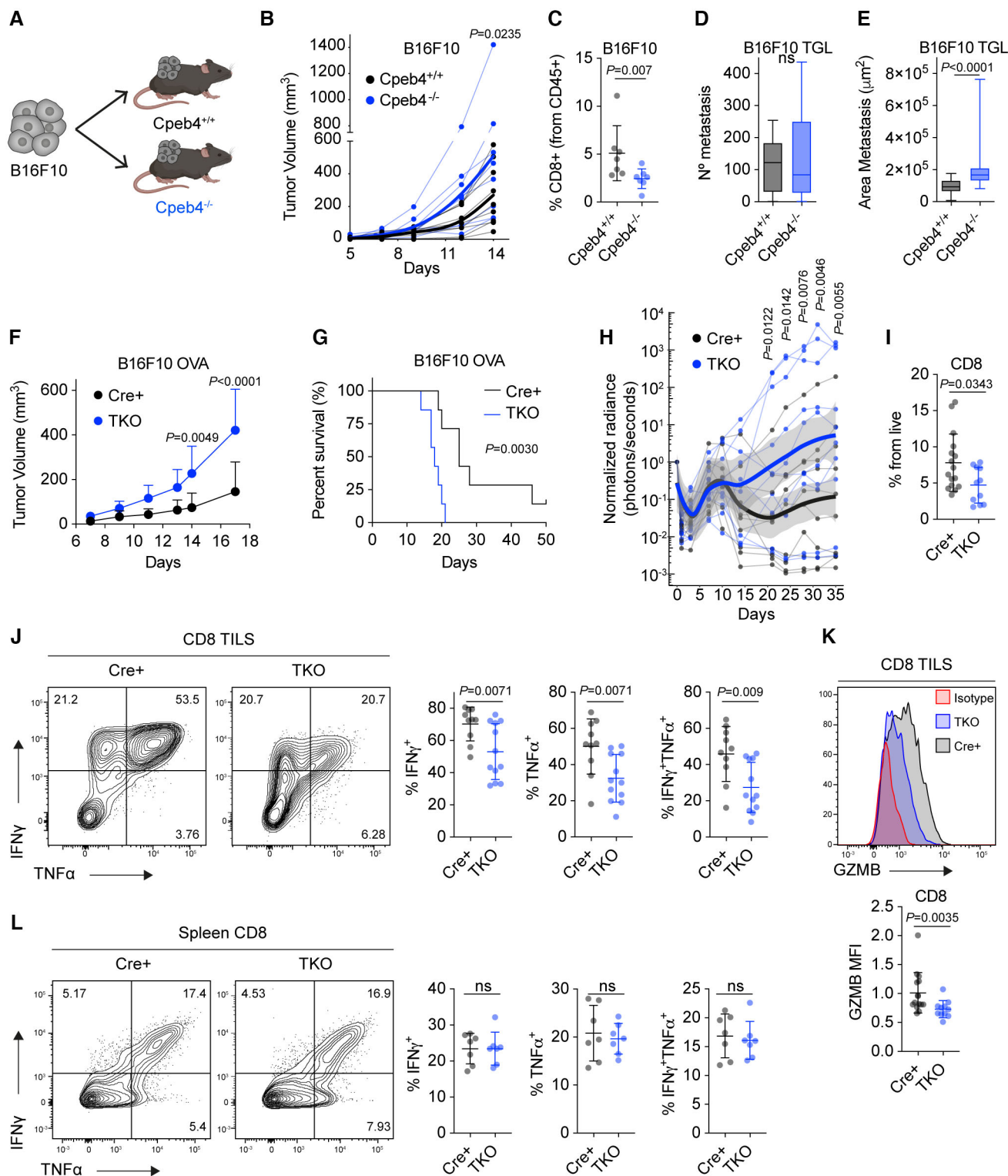
Figure 1.

tumor-infiltrating lymphocytes (TILs). Indeed, the percentage of IFNγ- and TNFα-producing CD8 and CD4 cells was reduced in TILs from CPEB4-TKO animals (Figs 1J and EV3D). CD8 TILs from TKO mice also had decreased levels of granzyme B (GZMB) production

(Fig 1K). In contrast, we observed no differences in splenic T cells between TKO and Cre+ mice (Figs 1L and EV3E), thereby indicating that the defects in effector molecule production were specific to TILs. This phenotype did not seem to originate in an exacerbated
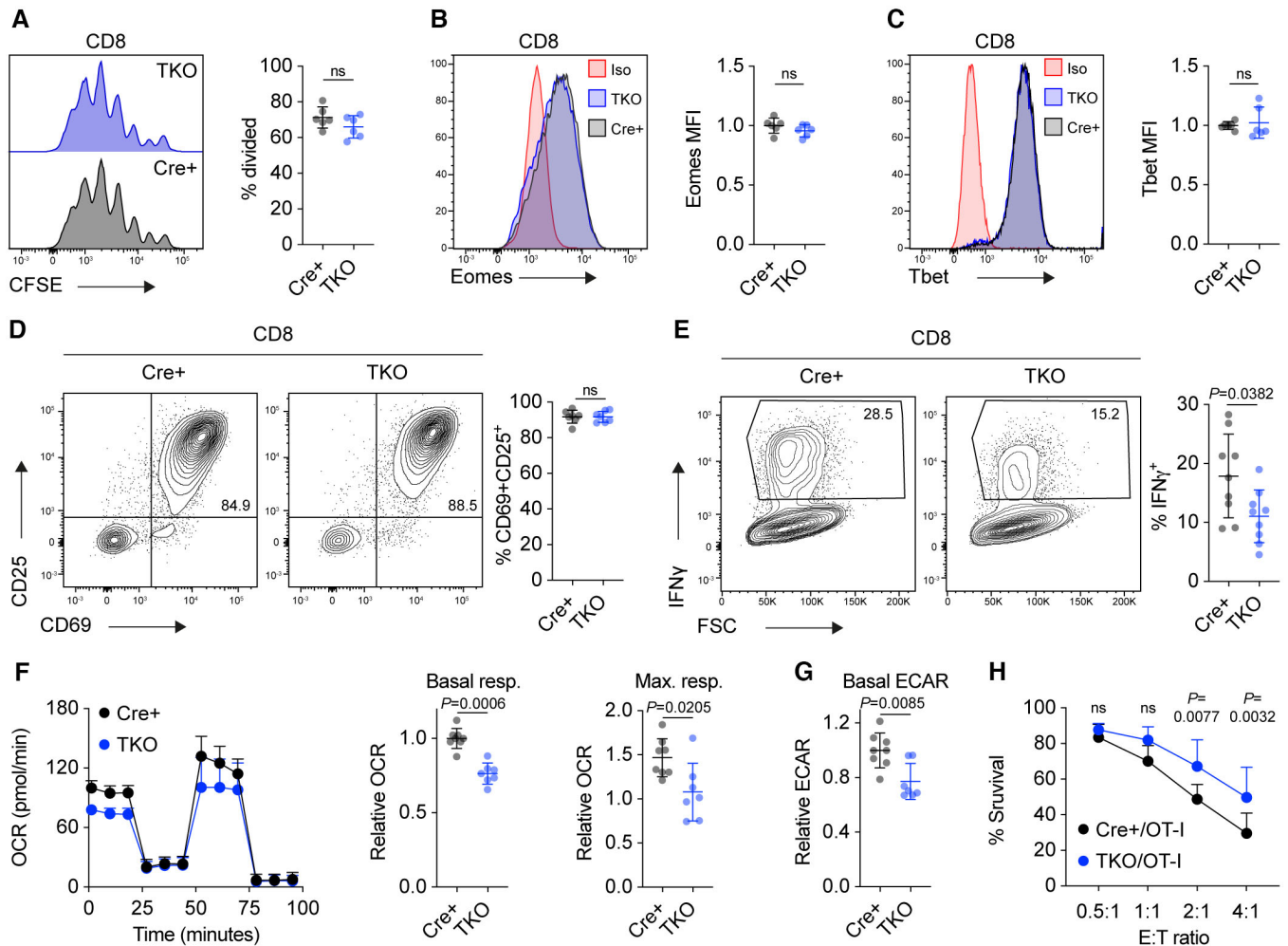
Figure 2. CPEB4 is required for T-cell effector function but not for early activation, proliferation, or induction of differentiation.

A   Proliferation assay of carboxyfluorescein succinimidyl ester (CFSE)-labeled CD8 T cells activated *ex vivo* with CD3/CD28/IL-2 for 72 h. CD8 T cells were isolated from spleen and lymph nodes of WT and TKO mice. Left: representative histogram of CD8 T-cell proliferation ($n = 6$ mice per genotype); right: quantification of the percentage of divided cells ($n = 6$ mice per genotype).

B, C   Representative histograms (left panels) and quantification (right panels) of Eomes (B) or Tbet (C) median fluorescent intensity (MFI) from Cre[+] or TKO CD8 T cells following activation with CD3/CD28/IL-2 for 48 h ($n = 6$ mice for each genotype). T cells were isolated as in (A). Values are normalized to Cre[+].

D   Representative flow cytometry plots (left panels) and quantification (right panel) of early activation markers CD25 and CD69 in CD8 cells activated *ex vivo* with CD3/CD28/IL-2 for 24 h ($n = 7$ mice per genotype). T cells were isolated as in (A).

E   Representative flow cytometry plots (left panels) and quantification (right panel) of IFNγ^{+} CD8 cells activated *ex vivo* as in (B) ($n = 9$ mice per genotype). T cells were isolated as in (A).

F   Oxygen consumption rate of Cre[+] ($n = 8$ mice) or TKO ($n = 7$ mice) CD8 T cells activated *ex vivo* as in (B) after mitochondrial stress test analysis. Two representative WT and TKO animals are shown (left panel); the corresponding quantification for basal and maximum respiration is shown (right panels). Values are normalized to basal Cre[+] measurements. T cells were isolated as in (A).

G   Extracellular acidification rate (ECAR) of Cre[+] ($n = 8$ mice) or TKO ($n = 7$ mice) CD8 T cells activated *ex vivo* as in (B) measured in basal conditions and normalized to Cre[+]. T cells were isolated as in (A).

H   Survival percentage of B16F10 OVA melanoma cells co-cultured with OVA/IL-2 preactivated Cre[+]/OT-I or TKO/OT-I cells at increasing ratios of effector:target cell. Survival was measured by flow cytometry 16 h after co-culture ($n = 4$ mice for 0.5:1, $n = 8$ mice for 1:1, 2:1, and 4:1).

Data information: Data are represented as mean ± s.d. Statistical analysis was performed by two-way ANOVA with Sidak correction (H) and Mann–Whitney test (A–G). Exact *P*-values are indicated in the graphs; ns = not significant. The data are representative of two independent experiments (B and C) or pooled from two to four independent experiments (A, D–H).

exhaustion, as markers such as TIM-3, LAG-3, and PD1 were largely unaffected (Fig EV3F and G). Additionally, we detected no changes in FOXP3^{+} regulatory T cells (Tregs) (Fig EV3H). Thus, these results indicated that T cells require CPEB4 to acquire the effector phenotype in the TME. This observation is consistent with a defective antitumor immune response and the increased tumor growth present in CPEB4 KO and TKO mice. In contrast, T-cell development does not appear to require CPEB4 activity.
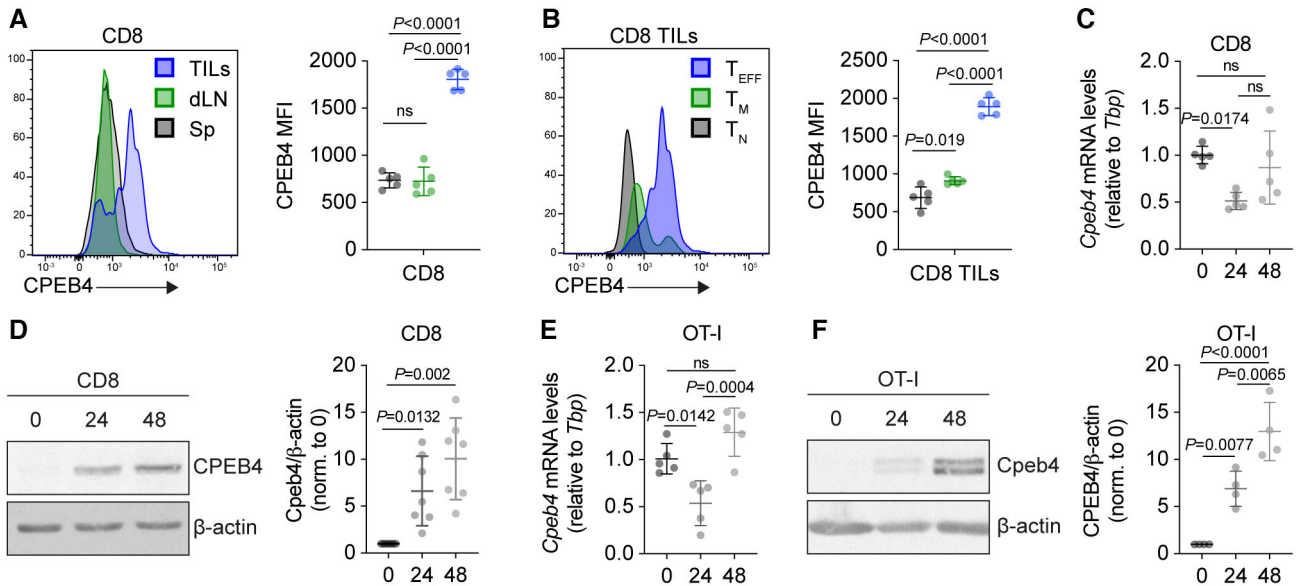
Figure 3. CPEB4 protein is upregulated in tumor-infiltrated effector CD8 T cells and upon T-cell activation *ex vivo*.

A Histogram (left panel) and quantification (right panel) of flow cytometric analysis of CPEB4 expression in CD8 T cells from spleen, draining lymph node, and B16F10 tumors ($n = 5$ mice).

B Histogram (left panel) and quantification (right panel) of CPEB4 MFI in naïve (T_N), effector (T_{eff}), and memory (T_M) CD8 TILs from B16F10 tumors ($n = 5$ mice).

C qPCR of *Cpeb4* mRNA in CD8 T cells resting or activated *ex vivo* with CD3/CD28/IL-2 at the indicated time points; *Tbp* is used as endogenous control ($n = 5$ mice). CD8 T cells were isolated from the spleen and lymph nodes from WT mice.

D Western blot (left panel) and quantification (right panel) of CPEB4 protein expression in CD8 resting or activated *ex vivo* with CD3/CD28/IL-2 at the indicated time points; β-actin is used as loading control ($n = 7$ mice). CD8 T cells were isolated as in (C).

E qPCR of *Cpeb4* mRNA in OT-I T cells resting or *ex vivo* activated with OVA/IL-2 at the indicated time points; *Tbp* is used as endogenous control ($n = 5$).

F Western blot (left panel) and quantification (right panel) of CPEB4 protein expression in OT-I T cells resting or activated *ex vivo* with OVA/IL-2 at the indicated time points; β-actin is used as loading control ($n = 4$).

Data information: Data are represented as mean ± s.d. Statistical analysis was performed by one-way ANOVA with Tukey correction (A–F). Exact *P*-values are indicated in the graphs; ns. = not significant. The data are representative of two to four independent experiments (A–F).
Source data are available online for this figure.

CPEB4 is required for T-cell effector function

Since T-cell activation and differentiation is a step-wise process that involves multiple molecular, metabolic, and cellular changes (Geltink *et al*, 2018), we sought to identify the stage at which CPEB4 is required for T-cell function. *Ex vivo* activated lymphocytes did not show defects in proliferation (Fig 2A), lineage specification (as defined by the expression of the effector T-cell identity transcription factors Tbet and Eomes; Fig 2B and C), or early activation (as defined by expression of CD25/CD69; Fig 2D). However, and in agreement with our *in vivo* observations (Fig 1), *ex vivo* activated TKO CD8 T cells produced less IFNγ (Fig 2E). These defects in IFNγ production were concomitant with the impairment of activated CD8 T-cell metabolic fitness, as reflected by decreased mitochondrial respiration (both basal and maximal levels) (Fig 2F) and reduced glycolysis (Basal ECAR, Fig 2G). To determine whether the defects in late activation events had functional consequences, we measured the cytotoxic capacity of CPEB4-depleted CD8 lymphocytes *ex vivo*. Indeed, TKO OT-I CD8 T cells showed reduced cytotoxic activity compared to WT T cells (Fig 2H), thereby indicating impaired functionality. Taken together, these results indicated that CPEB4 was required for the maintenance of the T lymphocyte effector

phenotype and fitness, independently of early activation, proliferation, or differentiation.

CPEB4 protein expression is induced in effector TILs and activated CD8 T cells

To further define a putative role of CPEB4 in TIL function, we measured whether CPEB4 expression was regulated upon T-cell activation. First, we determined whether activation caused changes in CPEB4 protein expression *in vivo* by comparing its levels in TILs to those in splenic and draining lymph node (dLN) CD8 and CD4 cells. Using a CPEB4-specific antibody for flow cytometry (Fig EV4A), we observed a strong upregulation of CPEB4 protein in CD8, but not CD4, TILs compared to splenic and dLN CD8 cells from tumor-bearing animals (Figs 3A and EV4B). When we compared CPEB4 expression among the CD8 TIL subsets, CPEB4 upregulation was specific to effector CD8 T cells but was not observed in naive or memory T cells (Figs 3B and EV4C). Subsequently, we purified CD8 T cells and activated them *ex vivo* with CD3 / CD28 / IL-2. While activation caused a reduction in *Cpeb4* mRNA levels at earlier time points (Fig 3C), CPEB4 protein was virtually undetectable in unstimulated CD8 cells and was expressed only upon activation (Fig 3D).

Although changes in protein stability cannot be ruled out, this apparent contradiction between mRNA and protein levels is frequently observed for mRNAs under strong translational control, such as *Cpeb4* mRNA (Maillo *et al*, 2017). To validate this *ex vivo* activation model, we also activated OT-I CD8 lymphocytes with OVA / IL-2, obtaining similar results (Fig 3E and F). In contrast, *Cpeb4* mRNA remained unaffected in *ex vivo* activated CD4 T cells, and CPEB4 protein upregulation was much lower compared to CD8 cells (Fig EV4D and E). Taken together, these results show that CPEB4 is post-transcriptionally upregulated in activated and effector CD8. Furthermore, in line with the observed phenotypes *in vivo* and *ex vivo*, CPEB4 upregulation is required to sustain T-cell effector function.

Loss of CPEB4 exacerbates terminal UPR in activated CD8 lymphocytes

To better understand the mechanistic basis for the phenotype observed in T-cell function, we compared the transcriptomes of CPEB4 WT and KO CD8 lymphocytes. In agreement with the negligible levels of CPEB4 in resting CD8 cells, non-activated lymphocytes displayed no differences between CPEB4 WT and KO conditions (Fig EV4F). In contrast, we detected differential expression of mRNAs from lymphocytes activated in the presence or absence of CPEB4 (Fig EV4G). Pathway enrichment analysis showed that the top categories that were differentially enriched in CPEB4-depleted cells corresponded to an increased unfolded protein response (UPR) (Fig 4A and B) and to anabolic pathways (MTORC1, Myc, Figs 4A, and EV4D and H). To functionally validate UPR upregulation in KO cells, we measured markers of ER stress. Indeed, eIF2α phosphorylation increased in activated CPEB4-depleted CD8 T cells as compared to WT cells (Fig 4C), as did the mRNA and protein levels of *Atf4*, *Ddit3* -CHOP-, and *Xbp1s mRNA* (Fig 4D and E). The levels of control mRNA *Hspa5* did not change under CPEB4 depletion. Accordingly, CPEB4-depleted CD8 TILs showed increased *Ddit3* mRNA levels when compared to splenic CD8 T cells (Figs 4F and EV4I). The upregulation of ER stress markers was concomitant with increased cell death (Fig 4F and G), suggesting that CPEB4 KO CD8 T cells underwent an exacerbated, maladaptive ER stress response upon activation.

CPEB4 directly mediates adaptation to ER stress in activated CD8 T cells

To identify the transcripts and pathways directly regulated by CPEB4 during the adaptation to functional ER stress in T cells, we performed CPEB4-RNA immunoprecipitation (RIP). As expected, mRNAs that co-immunoprecipitated with CPEB4 (Fig 5A) were enriched in CPEs (Fig 5B), thus indicating the specificity of the RIP method. In agreement with the global transcriptomic changes in CPEB4 KO cells, pathway analysis of direct CPEB4 targets showed enrichment in Myc and mTOR pathways, as well as in UPR signaling (Fig 5C), thereby suggesting that CPEB4 is a direct mediator of the integrated stress response in lymphocytes. Specifically, CPEB4 targets included genes required to suppress anabolism in response to stress (*Ddit4*, *Hyou1*), ubiquitination machinery (*Herpud2*), and ER translation machinery (*Tap1*, *Ssr2*, *Ssr3*) (Fig 5D and Table EV1). For DDIT4 and HERPUD2, we further validated that their protein

levels were reduced in the absence of CPEB4, without parallel changes in their respective mRNAs (Figs 5E and F, and EV5B and C). These observations thus suggest that CPEB4 functions as a translational activator in this context, which correlates with its hyperphosphorylated status (Fig EV5D) (Guillén-Boixet *et al*, 2016). It should be noted that neither the mRNAs encoding the main UPR sensors (*Eif2ak3* -PERK-, *Ern1* -IRE1α- and *Atf6*) nor the transcripts coding for mediators of the adaptive nor apoptotic responses (*Atf4*, *Xbp1*, *Ddit3* -CHOP-) were identified in the RIP (Fig 5D, Table EV1). We also ruled out direct CPEB4 regulation of the mRNAs encoding effector molecules (e.g., IFNγ, TNFα, GZMB) or effector T-cell master transcription factors (e.g., Eomes and Tbx21) (Fig EV5A, Table EV1).

CPEB4-dependent adaptation to ER stress sustains T-cell effector function

To link the maladaptation to ER stress with the defects in effector phenotypes, we activated control or CPEB4 TKO CD8 cells in the presence or absence of tauroursodeoxycholic acid (TUDCA, T), a chemical chaperone that attenuates ER stress (Keestra-Gounder *et al*, 2016). First, we measured metabolic fitness and IFNγ production. The alleviation of ER stress with TUDCA treatment rescued the metabolic fitness of CPEB4 KO cells, as reflected by the restoration of mitochondrial respiration (Fig 5G) and glycolysis (Fig 5H) to control levels. Similarly, IFNγ production in CPEB4 TKO cells was partially rescued by TUDCA (Fig 5I). Thus, maladaptation to ER stress in the absence of CPEB4 causes effector T-cell dysfunction. Next, we addressed whether CPEB4 induction upon CD8 activation was itself mediated by the UPR. To this end, we activated CD8 cells in the presence or absence of TUDCA and measured CPEB4 protein levels. TUDCA-treated cells showed a significant decrease in protein expression (Fig EV5E), without differences in *Cpeb4* mRNA levels (Fig EV5F). The phosphorylation of eIF2α suggests that CPEB4 synthesis in these cells could be induced through the translational bypass of its inhibitory upstream reading frames (uORFs) (Maillo *et al*, 2017). Of note, CD8 cells did not display differences in T-cell activation in the presence of TUDCA (Fig EV5G). Taken together, these results indicate that CPEB4 is an integral part of the UPR in T cells and that it is upregulated upon T-cell activation to promote cellular adaptation to activation-induced ER stress.

Discussion

A highly secretory phenotype elicits ER stress, which is caused by the accumulation of unfolded or misfolded proteins, thereby triggering the UPR. The UPR has three branches, which are mediated by transcription factor-6 (ATF6), inositol-requiring enzyme-1 α (IRE1α), and the eIF2α kinase PERK. eIF2α phosphorylation causes a global shutdown of protein synthesis. Concomitantly, eIF2α-phosphorylation allows for permissive translation of specific mRNAs carrying short uORFs. These early responses allow for the resolution of stress, or, when the stress cannot be resolved, they promote apoptosis by stimulating the synthesis of the transcription factor CHOP (Harding *et al*, 2000; Wek *et al*, 2006; Wang & Kaufman, 2014; Hetz *et al*, 2020). Therefore, these early responses have evolved to resolve transient acute stress. However, in physiological
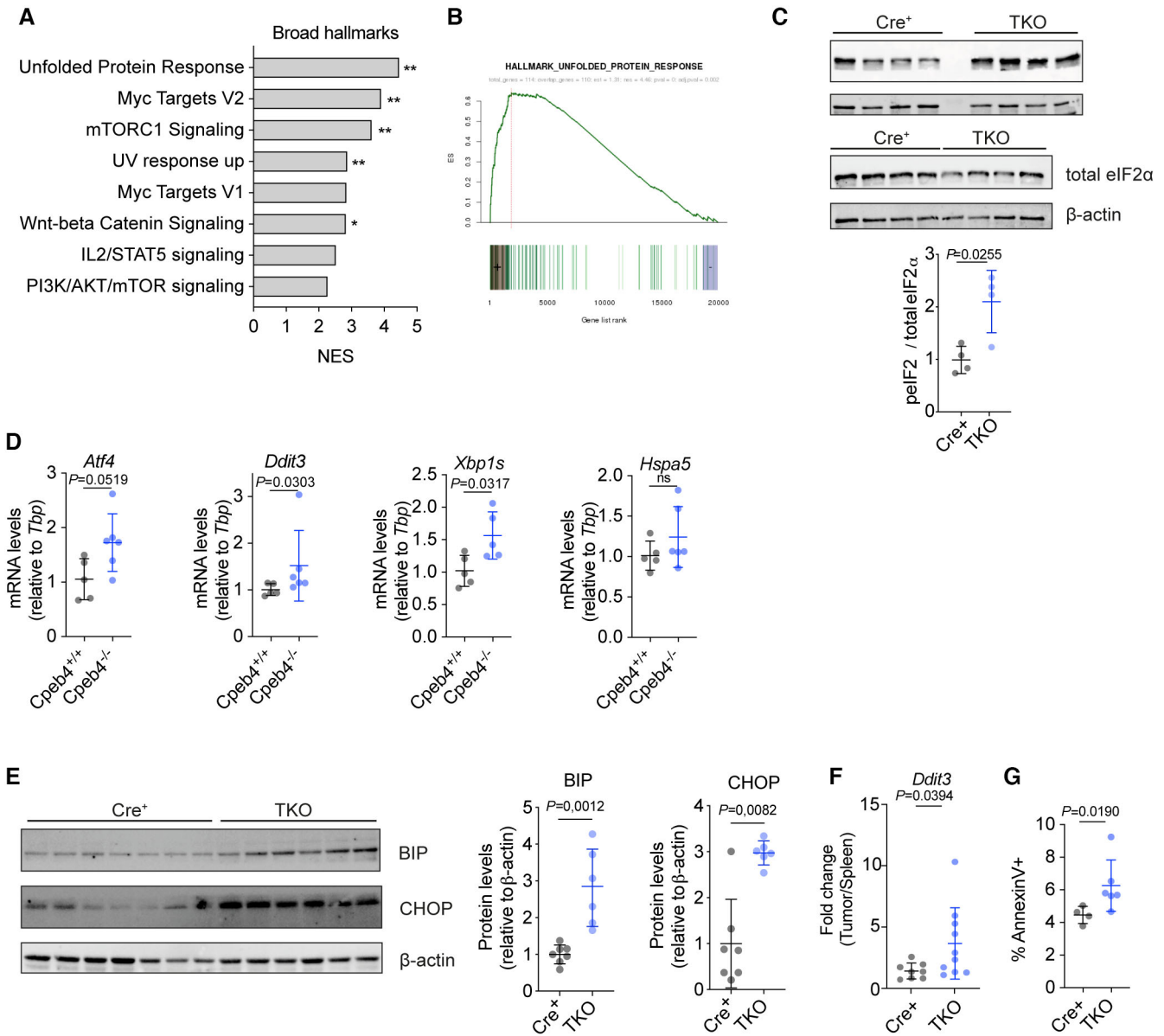
Figure 4. CPEB4 depletion leads to exacerbated UPR.

A Pathway enrichment analysis in Cpeb4$^{-/-}$ ($n = 3$) versus Cpeb4$^{+/+}$ ($n = 3$) CD8 cells activated *ex vivo* with CD3/CD28/IL-2 for 48 h. Top pathways enriched from the Molecular Signatures Database Hallmarks collection are shown. **AdjP = 0.002, *AdjP = 0.006.

B Enrichment plot of unfolded protein response gene set.

C Western blot analysis (upper panel) and quantification (lower panel) of eIF2α phosphorylation in WT ($n = 4$) and TKO ($n = 4$) CD8 T cells activated as in (A); total eiF2 α- and β-actin are used as loading control.

D qPCR analysis of *Atf4*, *Ddit3*, *Xbp1s*, and *Hspa5* mRNA levels in Cpeb4$^{+/+}$ ($n = 5$) and Cpeb4$^{-/-}$ ($n = 6$) CD8 cells activated as in a; *Tbp* is used as endogenous control ($n = 5$).

E Western blot analysis (left panel) and quantification (right panels) of BIP and CHOP proteins in WT ($n = 7$) and TKO ($n = 6$) CD8 T cells activated as in (A).

F *Ddti3* mRNA levels in CD8 T cells from B16F10 tumors and spleen of WT ($n = 8$) and TKO ($n = 10$) mice. The data are shown as ratio between tumors and spleen.

G Flow cytometry analysis of apoptotic AnnexinV$^+$ Cre$^+$ ($n = 4$) or TKO ($n = 6$) CD8 cells activated as in (A).

Data information: Data are represented as mean ± s.d. Statistical analysis was performed by the Mann–Whitney test (C–G). Exact *P*-values are indicated in the graphs, except for Fig A; ns = not significant. The data are representative of two independent experiments (C, F) or pooled from two to three independent experiments (D, E, G). Source data are available online for this figure.

scenarios, such chronic exposure of hepatocytes to a high-fat diet (HFD) probably causes milder but continued ER stress that cannot be resolved yet should not elicit an apoptotic response. At least in part, this chronic ER stress response is mediated by CPEB4, which activates the translation of CPE-containing mRNAs. The encoded factors, in turn, reduce metabolic ER stress in the absence of a

global translation shutdown. Thus, unlike eIF2α phosphorylation, the CPEB4-mediated response can be sustained for long periods without deleterious effects on the cell (Maillo *et al*, 2017). *Cpeb4*

mRNA translation is initially triggered by uORFs in its 5′ UTR (Maillo *et al*, 2017) and later sustained by CPEs in its 3′ UTR through a positive feedback loop (Igea & Mendez, 2010).
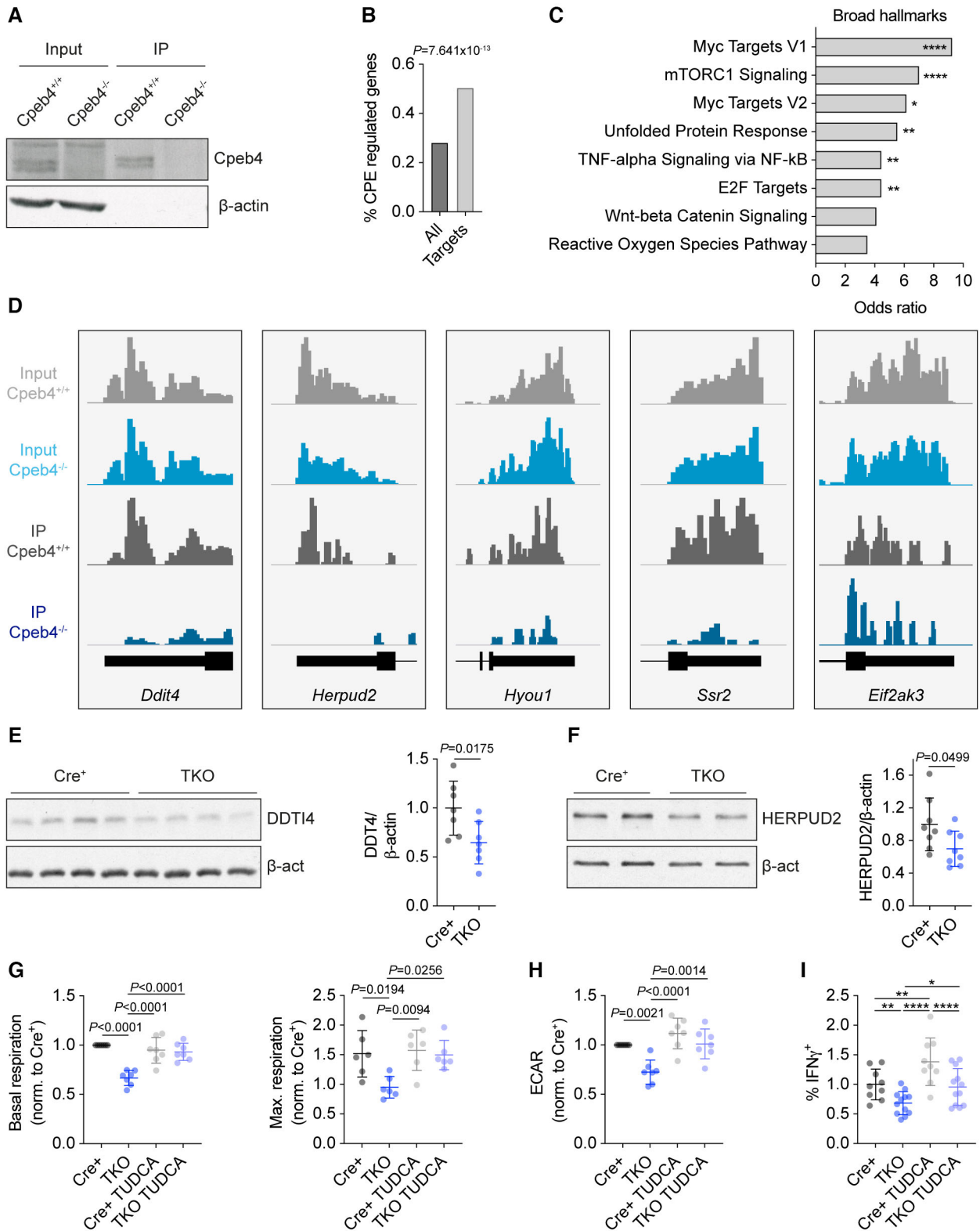

Figure 5.

◄

Figure 5. CPEB4-mediated adaptation to ER stress sustains T-cell effector function.

A   Western blot of CPEB4 in input and immunoprecipitated fractions using anti-CPEB4 antibody of Cpeb4$^{+/+}$ and Cpeb4$^{-/-}$ CD8 T cells activated *ex vivo* with CD3/CD28/IL-2 for 48 h; β-actin is used as control (*n* = 3).
B   Comparison of percentage of genes containing CPE element in their 3′UTR in the whole mouse transcriptome versus RIP targets.
C   Pathway enrichment analysis in CPEB4 RIP targets. Top pathways enriched from the Molecular Signatures Database Hallmarks collection database are shown, ordered by odds ratio. ****Adj*P* < 0.0001, **Adj*P* = 0.0038 (unfolded protein response), or Adj*P* = 0.0017 (TNFα signaling via NF-kB and E2F targets), *Adj*P* = 0.0315.
D   RIP-seq data from several 3′ UTRs depicting normalized RIP-seq coverage for inputs (light gray and blue) and IP (dark gray and blue) from Cpeb4$^{+/+}$ and Cpeb4$^{-/-}$ CD8 T cells. Image obtained using the integrated genome viewer (IGV).
E   Western blot (left panel) and quantification (right panel) of DDIT4 protein levels in Cre$^+$ and TKO CD8 T cells activated as in (A); β-actin is used as loading control (*n* = 7).
F   Western blot (left panel) and quantification (right panel) of HERPUD2 protein levels in Cre$^+$ and TKO CD8 T cells activated as in (A); β-actin is used as loading control (*n* = 8).
G   Basal oxygen consumption rate (left panel) and maximal oxygen consumption rate (right panel) after mitochondrial stress test analysis. Cre$^+$ and TKO CD8 T cells were activated as in (A), but were treated with either tauroursodeoxycholic acid (TUDCA, T) 250 μM or vehicle for the last 24 h. Values are normalized to basal Cre$^+$ measurements. *n* = 7 for all conditions in basal respiration; *n* = 6 for all conditions in maximal respiration.
H   Extracellular acidification rate (ECAR) in basal conditions for Cre$^+$ and TKO CD8 T cells activated and treated *ex vivo* as in (G) (*n* = 7). Values are normalized to basal Cre$^+$ measurements.
I   Quantification of IFNγ$^+$ CD8 cells activated and treated as in (G) (*n* = 9 for Cre$^+$ and *n* = 12 for TKO in both conditions). **P* = 0.0168, ***P* = 0.0014 for Cre$^+$ versus TKO, *P* = 0.0029 for Cre$^+$ versus Cre$^+$ TUDCA, ****P* < 0.0001.

Data information: Data are represented as mean ± s.d. Statistical analysis was performed by Fisher's exact test (B), one-way ANOVA with Tukey correction (G–I), and Mann–Whitney test (E, F). Exact *P*-values are indicated in the graphs, except for panels C and I; ns = not significant. In G–I, only significant comparisons are depicted. The data are representative of two to three independent experiments (A) or pooled from two to four independent experiments (E–I).
Source data are available online for this figure.

UPR signaling is initially required for T-cell expansion and differentiation (Scheu *et al*, 2006; Kamimura & Bevan, 2008; Thaxton *et al*, 2017; Yang *et al*, 2018). Our results indicate that CPEB4 is not required in this context. However, contrary to the CPEB4-mediated response, the initial acute ER stress response by IRE1α and PERK, when unresolved, activates the XBP1s / CHOP-dependent terminal UPR with detrimental effects on antitumor immunity. Thus, genetic ablation of IRE1α or XBP1 in T cells enhances antitumor immunity, with increased IFNγ$^+$ CD4 T cells and reduced tumor growth (Song *et al*, 2018). Chemical or genetic inhibition of IRE1α signaling reduces cholesterol-induced upregulation of exhaustion markers and enhances antitumor immunity (Ma *et al*, 2019). Additionally, PERK-CHOP activation impairs T-cell function and, accordingly, knocking out CHOP or PERK in T cells enhances T-cell antitumor immunity (Cao *et al*, 2019).

We found that, unlike the early mediators of the acute ER stress response, CPEB4 is dispensable for T-cell expansion and differentiation. During the acquisition of the T-cell effector phenotype, CPEB4 is required to attenuate ER stress caused by sustained high anabolic and secretory activity. This phenotype is in apparent contrast to what has been described for the early mediators of the acute ER stress response, thereby suggesting that CPEB4 adaptive response is decoupled from terminal UPR. Accordingly, CPEB4 does not directly regulate the expression of T-cell effector function mediators such as *Ifnγ*, *Tnfα*, and *GzmB*. Instead, the production of these mediators is controlled by the stress adaptation mechanisms activated through the CPEB4-mediated chronic UPR branch. We show that CPEB4 synthesis is translationally induced upon T-cell activation concomitantly with the initial UPR response, presumably through eIF2α phosphorylation and permissive translation of uORF-containing mRNAs (Maillo *et al*, 2017). Taken together, our results are consistent with a model in which sustaining the chronic adaptive response to ER stress through CPEB4 avoids the detrimental effects of the terminal UPR, expected from the global translation inhibition caused by sustained eIF2α phosphorylation and subsequent CHOP activation. Therefore, CPEB4 function allows effector CD8 T cells to maintain their high anabolic and secretory capacity, and, consequently, their antitumor activity.

Materials and Methods

Mice

Ubiquitous, constitutive CPEB4 KO mice (Cpeb4$^{-/-}$) and Cpeb4$^{lox/lox}$ mice were previously described (Calderone *et al*, 2016; Maillo *et al*, 2017). T cell-specific CPEB4 knockout mice (CPEB4-TKO) were obtained by crossing Cpeb4$^{lox/lox}$ mice with CD4-Cre transgenic animals (Lee *et al*, 2001) from Jackson and were maintained in pure C57BL6/J background. Cpeb4$^{-/-}$ mice were backcrossed for seven generations onto the C57BL/6J background. OT-I mice were obtained from Jackson. To generate CPEB4-TKO/OT-I mice, OT-I mice were crossed with CPEB4-TKO mice. Mice were maintained in a specific pathogen-free (SPF) facility under a 12-h light–dark cycle and given *ad libitum* access to a standard diet and water. Animals were used at 7–12 weeks of age with sex- and age-matched controls. All animal experiments were approved by the Animal Care and Use Committee of Barcelona Science Park (CEEA-PCB) and the Government of Catalonia.

Cell lines

The B16F10 murine melanoma cell line was obtained from ATCC. B16F10 cells expressing OVA-GFP were provided by D. Sancho and have been described previously (Sancho *et al*, 2008). B16F10 TGL cells were generated by infecting B16F10 cells with retrovirus containing the TGL (Thymidine kinase-GFP-Luciferase, provided by R. Gomis) plasmid. Briefly, HEK–293T cells were transfected with TGL vector and plasmids encoding retroviral particles using standard methods. B16F10 cells were subjected to two consecutive rounds of infection and expanded for 7 days without selection. At day 7, GFP$^+$ cells were isolated by fluorescence-activated cell sorter

(FACS) and expanded. Cells were cultured in DMEM d-glucose medium (Gibco) supplemented with 10% fetal bovine serum, 1% penicillin/streptomycin, and 2 mM L-glutamine (Gibco). Mouse colorectal tumor organoids (MTOs) carrying patient-specific oncogenic mutations and expressing luciferase have been previously described (Tauriello et al, 2018).

In vivo tumor studies

For subcutaneous tumor growth, 2×10^5 B16F10 or 2.5×10^5 B16F10 OVA-GFP cells were injected into the flanks of sex-matched, 8- to 12-week-old mice (0.05, 0.2, 0.5×10^6 B16F10 cells were used to set up the best condition). Tumors were allowed to grow for 14 days except in experiments where survival curves were calculated. Survival time was defined as the time required for a tumor to reach a volume of 500 mm³, which is the humane endpoint approved by our Ethics committee. Tumor dimensions were measured 2–3 times a week with a digital caliper, and tumor volume was calculated by applying the following formula: Volume = length × width² / 2. For melanoma experimental metastasis assays, 4×10^5 B16F10 TGL cells were injected in 100 µl of PBS into lateral tail veins and were allowed to grow for 14 days. For liver colonization experiments, intrasplenic injections of MTOs were performed as previously described (Tauriello et al, 2018). Briefly, MTOs cultured in standard conditions were dissociated with trypsin into a single-cell suspension and injected at a ratio of 500 k cells per animal. MTOs were injected in C57BL/6J hosts aged 7–8 weeks, sex-matched with the organoid injected. The growth kinetics of luciferase-expressing melanoma or colorectal cancer organoids were monitored with in vivo bioluminescence using an IVIS Spectrum (Perkin-Elmer). Mice were anesthetized before receiving a retroorbital injection of 50 µl D-luciferin at 15 mg/ml (Resem BV). Total photon flux measurements were normalized per mouse to day 0 post-injection values. Metastatic foci at the endpoint of the experiment were counted manually. For melanoma lung metastasis, the area of each nodule was measured on H&E sections with QPath 0.2.3.

Tumor, spleen, lymph node, thymus, and blood processing

Tumors were minced in RPMI containing 0.5 mg/ml collagenase I (Sigma Aldrich) and 20 µg/ml DNase I (Roche) and incubated in a gentleMACS Octo Dissociator with Heaters (Miltenyi Biotec) using the program 37C_m_TDK_1. Samples were then filtered through a 70 µm cell strainer and washed with 2% FBS HBSS (FACS buffer) to obtain a single-cell suspension. Spleen, thymus, and lymph nodes were mechanically processed into a single-cell suspension. Blood was collected and supplemented with 50 mM EDTA to prevent coagulation. Erythrocytes were lysed using an isotonic ammonium chloride solution before performing antibody staining.

Flow cytometry analysis

Prior to antibody staining, single-cell suspensions were incubated with TruStain fcX™ (anti-mouse CD16/32) antibody (1:100, #101320, Biolegend) for 10 min on ice. For cell surface staining, cells were incubated for 20 min on ice with the following antibodies: anti-CD45 BV605 (clone 30-F11, 1:400, #103139, Biolegend); anti-CD3ε PerCPCy5.5 (clone 145-2C11, 1:100, # 100327,

Biolegend); anti-CD4 APC-eFluor780 (clone GK1.5, 1:200, #47–0041-80, eBiosciences); anti-CD4 FITC (clone GK1.5, 1:200, #11-0041-81, eBiosciences); anti-CD8 BV786 (clone 53-6.7, 1:400, #563332 BD Biosciences); anti-CD8 FITC (clone 53–6.7, 1:400, #100705, Biolegend); anti-CD44 PE (clone IM7, 1:200, #103023, Biolegend); anti-CD44 APC (clone IM7, 1:200, #103011, Biolegend); anti-CD11b FITC (clone M1/70, 1:200, #553310 BD Biosciences); anti-CD69 FITC (clone H1.2F3, 1:200, # 104505, Biolegend); anti-CD25 PE-Cy7 (clone PC61.5, 1:300, # 25-0251-81, eBiosciences); anti-CD25 APC (clone PC61.5, 1:300, # 17-0251-81, eBiosciences); anti-CD62L PE-Cy7 (clone MEL-14, 1:200, #25-0621-81, eBiosciences); anti-TIM3 PE (clone RMT3-23, 1:100, #119703, Biolegend); anti-LAG-3 APC (clone C9B7W, 1:100, #125209, Biolegend); and anti-PD-1 PE (clone 29F.1A12, 1:200, #135,205, Biolegend).

For CPEB4 intracellular staining, T cells were enriched with density gradient centrifugation (800 g, 30 min) at 25°C with 40 and 80% Percoll (GE Healthcare). Cells were labeled with surface antibodies followed by fixation/permeabilization with Cytofix/Cytoperm kit (BD Biosciences). Cells were then blocked with permeabilization buffer containing 10% donkey serum (Merk) and 2% BSA for 30 min on ice. Cells were then incubated with anti-CPEB4 (Mouse Monoclonal ERE149C, 1:100, homemade) diluted in permeabilization buffer with 2% donkey serum and 2% BSA for 30 min at room temperature. They were subsequently incubated with donkey anti-mouse AF647 (1:1,000, #A32787TR, Invitrogen) for 30 min on ice. The specificity of the antibody was confirmed by performing the staining with CPEB4 KO cells.

For cytokine intracellular staining, cells were restimulated in vitro with 50 ng/ml Phorbol 12-myristate 13-acetate (PMA, Sigma), 1 µg/ml ionomycin (Sigma), and Golgiplug inhibitor (1:1,000, BD Biosciences) for 3 h. Surface antigens were labeled before fixation/permeabilization with Cytofix/Cytoperm kit (BD Biosciences), followed by incubation with anti-IFNγ APC (clone XMG1.2, 1:200, #505809, Biolegend), anti-TNFα PE (clone MP6-XT22, 1:200, #506305, Biolegend), and anti-Granzyme B PE (clone NGZB, 1:200, # 12-8898-80 eBiosciences).

For transcription factor staining, fixation/permeabilization was performed with FOXP3 / Transcription Factor Staining Buffer Set (eBiosciences) after surface staining. Anti-FOXP3 PE (clone FJK-16s, 1:100, # 12-5773-80, eBiosciences), anti-TBET APC (clone 4B10, 1:100, #644813, Biolegend), and anti-Eomes PE (clone Dan11mag, 1:100, #12-4875-80, eBiosciences) were used.

For apoptotic cell analysis, cells were stained with AnnexinV-Cy5 (BD. Biosciences) following the manufacturer's instructions.

FACS analyses were performed using a FACS Aria Fusion (BD Biosciences) with BD FACSDiva software (v.8.0.1). Data were analyzed using FlowJo. DAPI or LIVE/DEAD™ Fixable Violet Dead Cell Stain Kit (Thermo Fisher) was used to exclude dead cells in non-fixed/fixed cells, respectively.

Immunohistochemistry and immunofluorescence

Tumors and lungs were fixed in a 10% neutral buffered formalin solution and embedded in paraffin. Three micrometer sections were air-dried and further dried overnight at 60°C. Antigen retrieval was performed with Tris-EDTA buffer (pH 9) using a PT Link (Dako). Endogenous peroxidase was quenched by 10 min incubation with peroxidase blocking solution (Dako REAL, S2023). For CD3 IHC,

anti-CD3 antibody (1:100, #IS50330, Dako) was incubated for 2 h at room temperature. A biotin-free, ready-to-use BrightVision poly–horseradish peroxidase (HRP)–anti-rabbit immunoglobulin G (Immunologic, DPVR-110HRP) was used as secondary antibody. Sections were counterstained with hematoxylin (Dako, S202084) and mounted with toluene-free mounting medium (Dako, CS705). For immunofluorescence, anti-CD8 (1:1,000, #ab217344, Abacam), anti-CD31 (1:300, #ab28364, Abcam), and anti-CD140a (1:100, #AF1062, R&D) were incubated overnight at 4°C and Alexa secondary antibodies and DAPI were used. Images were acquired with a NanoZoomer-2.0 HT C9600 scanner (Hamamatsu). Image analysis was performed using QPath 0.2.3.

Mouse T-cell culture and *ex vivo* activation

Spleen and lymph nodes from WT, Cpeb4$^{-/-}$, and CPEB4-TKO mice were mechanically processed into a single-cell suspension. CD8 or CD4 T cells were purified using Dynabeads™ FlowComp™ Mouse CD8 Kit (Themo Fisher) or Dynabeads™ FlowComp™ Mouse CD4 Kit (ThemoFisher), respectively. Isolated cell purity was confirmed by flow cytometry (> 95%). T cells were cultured in RPMI medium (Gibco) supplemented with 10% Fetal Bovine Serum, 1% penicillin/streptomycin, 2 mM L-glutamine (Gibco), 1 mM sodium pyruvate (Gibco), and 55 μM β-mercaptoethanol at 37°C, 5% CO_2, and 5% O_2. Purified T cells were activated with 1 μg/ml anti-CD3 antibody (clone 145-2C11, #MA5-17655, Thermo Fisher), 1 μg/ml anti-CD28 antibody (clone CD28.6, #16-0288-85, eBiosciences), and 20 ng/ml IL-2 (212-12, PeproTech) for the indicated periods. OT-I WT and CPEB4-TKO splenocytes were processed into a single-cell suspension and plated into T-cell media supplemented as described above. For OT-I activation, 1 μg/ml OVA$_{257-264}$ peptide (vac-sin, InvivoGen) and 20 ng/ml IL-2 were added to the media. Activated OT-I CD8 cells were purified at the indicated time points for downstream analysis by either Dynabeads™ or FlowComp™ Mouse CD8 Kit.

Immunoblotting

Cells were lysed in ice-cold radioimmunoprecipitation assay (RIPA) lysis buffer supplemented with phosphatase and protease inhibitors, and protein concentration was determined using the DC Protein assay (Bio-Rad). Equal amounts of proteins were separated by SDS–polyacrylamide gel electrophoresis and transferred onto nitrocellulose membranes (Sigma) for 1 h at 400 mA. Membranes were blocked in 5% milk and incubated with antibodies against CPEB4 (Mouse Monoclonal ERE149C, 1:500, homemade), β-Actin-HRP (1:15,000, ab49900, Abcam), vinculin (1:1,000, ab130007 Abcam), DDIT4 (1:1,000, 10,638-1-AP, Proteintech), HERPUD2 (1:500, sc-398583, Santa Cruz), phospho-eiF2α (s51) (1:1,000, ab32157, Abcam), total eiF2α (1:1,000, 9722S, Cell Signaling), CHOP (1:1,000, CST5554T, Cell Signaling), and BiP (1:1,000, C50B12, Cell Signaling).

Lambda protein phosphatase assay (l-PPase)

Primary CD8 cells were isolated and activated as explained above. At 48 h post-activation, cells were lysed with l-PPase reaction buffer (New England BioLabs, Ipswich, MA) supplemented with 0.4% NP-40 and EDTA-free protease inhibitors (Sigma-Aldrich). The phosphatase reaction was performed following the manufacturer's instructions.

Proliferation analysis by CFSE staining

CFSE (Invitrogen) staining was performed following the manufacturer's instructions. Briefly, 1×10^6 purified CD8$^+$ T cells were resuspended in 1 ml of PBS containing 1 μM CFSE (Thermo Fisher). Cells were incubated for 20 min at 37°C, and staining was stopped by adding five volumes of cell culture medium. Cells were washed and activated as described above. After 3 days, cells were analyzed by flow cytometry.

Ex vivo cytotoxicity assay

WT and TKO OT-I CD8 T cells were activated as described above, and 48 h after activation T cells were purified by the Percoll density gradient. OT-I cells were subsequently co-culture with a mix of 50% B16F10 OVA-GFP target cells labeled with 5 μM CFSE and 50% B16F10, non-target cells labeled with 1 μM CellTrace Far Red (Thermo Fisher) at different effector:target ratios (0.5:1, 1:1, 2:1, and 4:1) maintaining tumor cell number constant. After 16 h, tumor cell viability was examined by flow cytometry comparing the % of CFSE$^+$ and far red$^+$ cells. Cell survival percentage was calculated as % survival = 100 × (sample % target cell ÷ sample % non-target cell) ÷ (control % target ÷ control % non-target cell). Tumor cells cultured without OT-I cells were used as controls.

Seahorse analysis

OCR and ECAR were measured using an XFe24 extracellular flux analyzer (Seahorse Bioscience). CD8 T cells were activated with CD3/CD28/IL2 for 48 h, and then washed and plated onto poly-L-lysine (0.5 μg/ml, Sigma Aldrich)-coated XFe24 plates (3×10^5 cells/well). Cells were subjected to a Seahorse XF Cell Mito Stress Test using non-buffer XF RPMI medium supplemented with 10 mM glucose, 2 mM glutamine, and 1 mM sodium pyruvate (all from Agilent technologies). OCR was measured in basal conditions and after sequential addition of 1 μM oligomycin, 1 μM carbonyl cyanide p-trifluoromethoxyphenylhydrazone (FCCP), and 100 nM rotenone plus 1 μM antimycin A (Rot + AA). Basal and maximal respiration was calculated by subtracting non-mitochondrial respiration (Rot + AA values) from basal or FCCP-mediated respiration respectively. Maximal respiration values were normalized to basal respiration. ECAR was measured in basal conditions.

Tauroursodeoxycholic acid (TUDCA) treatments

For ER stress-dependent CPEB4 protein upregulation experiments, 250 μM TUDCA or vehicle was added to CD8 cells 2 h after activation. Cells were harvested 24 h after activation. For seahorse experiments, 250 μM TUDCA was added for the last 24 h of a 48 h activation period.

RT–qPCR analysis

Total RNA was extracted by TRIzol reagent (Invitrogen), followed by DNAse treatment (Ambion). 500–100 ng of RNA was then

retrotranscribed into cDNA using random hexamers with Super-Script IV (Thermo Fisher). Quantitative real-time PCR was performed in a QuantStudio 6 Flex (Applied Biosystems) using PowerUp SYBR Green Master Mix (Thermo Fisher). RNA quantifications were normalized to *Tbp* as endogenous control. The primers used are listed in Table EV2.

RNA-seq

Resting or 48 h-activated Cpeb4$^{+/+}$ and Cpeb4$^{-/-}$ primary CD8 were harvested and washed twice with PBS. RNA was then extracted as explained above. Samples were processed at IRB Barcelona's Functional Genomics Facility, following standard procedures, and libraries were sequenced by Illumina 50 bp single end. Reads were aligned against the UCSC mm10 genome with STAR 2.7.0a (Dobin *et al*, 2013) and default options. Counts at the gene level (Ensembl GRC.m38.07) were obtained using featureCounts with default options. DESeq2 1.22 was used to detect differentially expressed genes between groups of interest using Benjamini–Hochberg adjusted *P*-values (Love *et al*, 2014). For gene set enrichment analysis, it was performed a regularized log transformation (rlog) applied to the count data using the DESeq2 R package 1.22, with the Roast (Wu *et al*, 2010) method using the MaxMean statistic. Hallmark gene set was obtained from the Broad Institute MSigDB website (Liberzon *et al*, 2015) and mapped from human to mouse genes using homology information from Ensembl biomart archive in July 2016.

RNA-immunoprecipitation (RIP) sequencing

A total of 30–40 million Cpeb4$^{+/+}$ and Cpeb4$^{-/-}$ primary CD8 cells (pooled from three to four animals) were isolated and activated as described above for 48 h in biological triplicates. Activated CD8 cells were harvested, washed twice with 15 ml of cold PBS, and incubated in 15 ml of FBS-free, 0.5% formaldehyde DMEM for 5 min at room temperature with soft agitation to allow crosslinking of RNA-binding proteins to target RNAs. Crosslinking was quenched by adding 5 ml of 1 M glycine for 5 min. Cells were washed twice with cold PBS, lysed in 1 ml of RIPA buffer (25 mM Tris-Cl pH7.6, 1% Nonidet P-40, 1% sodium deoxycholate, 0.1% SDS, 100 mM EDTA, and 150 mM NaCl) containing protease inhibitors and RNase inhibitors, and then sonicated for 5 min at low intensity with a Standard Bioruptor Diagenode. Extracts were precleared and immunoprecipitated (overnight, 4°C on rotation) with 30 µg of anti-CPEB4 antibody (Mouse Monoclonal ERE149C, homemade) bound to 150 µl of Dynabeads Protein G (Invitrogen). Beads were washed five times with cold RIPA buffer supplemented with Protease inhibitors. For protein extraction, beads were resuspended in 100 µl proteinase-K buffer with 70 µg of proteinase-K (Roche) and incubated for 60 min at 65°C. RNA was extracted by standard phenol–chloroform, followed by Turbo DNA-free Kit (Ambion) treatment. Samples were processed at the IRB Functional Genomics Facility following standard procedures and libraries were sequenced by Illumina 50 bp single end. Reads from Cpeb4$^{+/+}$ and Cpeb4$^{-/-}$ CD8 inputs and IPs in biological triplicates were aligned against UCSC mm10 rRNA genome (October 2016) to identify rRNA-contaminated reads with Bowtie1 using default options (Langmead *et al*, 2009). Non-rRNA reads (Bowtie1 unmapped) were then aligned against the UCSC mm10 genome with Bowtie 2 using the default option

(Langmead & Salzberg, 2012). TDF files for visual inspection were generated with IGVTools 2 (Thorvaldsdottir *et al*, 2013). 3′ UTR coordinates for the mm10 genome were obtained from Ensembl Biomart (March 2017). 3′ UTR counts were generated with R 3.5.1 and featureCounts from RSubread v1.32.4 (Liao *et al*, 2019) with options allowMultiOverlap = TRUE, countMultiMappingReads = FALSE, and minMQS = 1 over mm10 3′ UTR regions. CPEB4 targets were defined by an interaction analysis of Cpeb4$^{+/+}$ and Cpeb4$^{-/-}$ RIP samples and their respective input controls (Cpeb4$^{+/+}$IP/ Cpeb4$^{+/+}$ Input vs. Cpeb4$^{-/-}$IP/Cpeb4$^{-/-}$Input) using DESeq2 (Love *et al*, 2014), with raw *P*-value < 0.05 and fold change > 1.5 as thresholds. Gene set enrichment for selected targets was performed using the online Enrichr tool (November 5, 2020) (Kuleshov *et al*, 2016). For the analysis of CPE-A-containing mRNAs, the script developed by Pique *et al* (2008) was run over mm10 3UTR reference sequences (Biomart Ensembl archive February 2014).

Statistics and reproducibility

Data are represented as mean ± SD unless otherwise stated in the figure legend. Statistics were analyzed with GraphPad Prism software. For two-group comparison, the Mann–Whitney test; for multiple comparisons, one- or two-way ANOVA with Sidak correction; and for survival, the Log-rank (Mantel-Cox) test were performed. A linear model with random effects was used for *in vivo* growth of colorectal cancer liver metastasis. Fisher's exact test was used to determine CPE enrichment in RIP-seq IP fractions. *P*-values < 0.05 were considered significant. Exact *P*-values are provided; in those cases where *P*-values are indicated with an asterisk, exact *P*-values are provided in the figure legend. For animal studies, aged- and sex-matched animals were used. The experiment was blinded before and during experimental analysis. Littermates were used whenever possible, and animals from different groups were kept in the same cage. No statistical test was used to determine sample size up front. The sample size was determined empirically according to previous knowledge of the variation in experimental setup. No data were excluded from the analysis. Experiments were repeated independently with similar results as indicated in the figure legend.

Data availability

The mouse models and materials generated for this work can be provided by the authors pending scientific review and completed material transfer agreement. All data needed to evaluate the conclusions in the paper are present in the paper and/or Expanded View. The RNA-seq and RIP-seq datasets generated and analyzed during the current study have been deposited at https://www.ncbi.nlm. nih.gov/geo/ (series number GSE189766, https://www.ncbi.nlm. nih.gov/geo/query/acc.cgi?acc = GSE189766). Additional data related to this paper can be requested from the authors.

Author contributions

Marcos Fernández-Alfara: Conceptualization; resources; formal analysis; supervision; investigation; writing – original draft; writing – review and editing. **Annarita Sibilio:** Resources; formal analysis; investigation; methodology; writing – review and editing. **Judit Martin:** Formal analysis; investigation. **Elsa Tusquets Uxó:** Resources; formal analysis; investigation; methodology. **Marina Malumbres:** Resources; formal analysis; investigation; methodology. **Victor Alcalde:** Formal analysis; investigation. **Verónica Chanes:** Formal analysis; investigation; methodology. **Adriá Cañellas-Socias:** Resources; formal analysis; investigation; methodology. **Sergio Palomo-Ponce:** Formal analysis; investigation. **Eduard Battle:** Resources; supervision; funding acquisition. **Raúl Méndez:** Conceptualization; supervision; funding acquisition; writing – original draft; writing – review and editing.

Disclosure and competing interests statement

The authors declare that they have no conflict of interest.

References

Calderone V, Gallego J, Fernandez-Miranda G, Garcia-Pras E, Maillo C, Berzigotti A, Mejias M, Bava FA, Angulo-Urarte A, Graupera M *et al* (2016) Sequential functions of CPEB1 and CPEB4 regulate pathologic expression of vascular endothelial growth factor and angiogenesis in chronic liver disease. *Gastroenterology* 150: 982 – 997

Cao G, Chen D, Liu G, Pan Y, Liu Q (2018) CPEB4 promotes growth and metastasis of gastric cancer cells via ZEB1-mediated epithelial-mesenchymal transition. *Onco Targets Ther* 11: 6153 – 6165

Cao Y, Trillo-Tinoco J, Sierra RA, Anadon C, Dai W, Mohamed E, Cen L, Costich TL, Magliocco A, Marchion D *et al* (2019) ER stress-induced mediator C/EBP homologous protein thwarts effector T cell activity in tumors through T-bet repression. *Nat Commun* 10: 1280

Chang CH, Qiu J, O'Sullivan D, Buck MD, Noguchi T, Curtis JD, Chen Q, Gindin M, Gubin MM, van der Windt GJ *et al* (2015) Metabolic competition in the tumor microenvironment is a driver of cancer progression. *Cell* 162: 1229 – 1241

Chen X, Cubillos-Ruiz JR (2021) Endoplasmic reticulum stress signals in the tumour and its microenvironment. *Nat Rev Cancer* 21: 71 – 88

Dobin A, Davis CA, Schlesinger F, Drenkow J, Zaleski C, Jha S, Batut P, Chaisson M, Gingeras TR (2013) STAR: ultrafast universal RNA-seq aligner. *Bioinformatics* 29: 15 – 21

Elia I, Haigis MC (2021) Metabolites and the tumour microenvironment: from cellular mechanisms to systemic metabolism. *Nat Metab* 3: 21 – 32

Fabbri L, Chakraborty A, Robert C, Vagner S (2021) The plasticity of mRNA translation during cancer progression and therapy resistance. *Nat Rev Cancer* 21: 558 – 577

Fernandez-Miranda G, Mendez R (2012) The CPEB-family of proteins, translational control in senescence and cancer. *Ageing Res Rev* 11: 460 – 472

Geltink RIK, Kyle RL, Pearce EL (2018) Unraveling the complex interplay between T cell metabolism and function. *Annu Rev Immunol* 36: 461 – 488

Guan BJ, van Hoef V, Jobava R, Elroy-Stein O, Valasek LS, Cargnello M, Gao XH, Krokowski D, Merrick WC, Kimball SR *et al* (2017) A unique ISR program determines cellular responses to chronic stress. *Mol Cell* 68: 885 – 900

Guillén-Boixet JB, Buzon V, Salvatella X, Méndez R (2016) CPEB4 is regulated during cell cycle by ERK2/Cdk1-mediated phosphorylation and its assembly into liquid-like droplets. *Elife* 5: e19298

Harding HP, Zhang Y, Bertolotti A, Zeng H, Ron D (2000) Perk is essential for translational regulation and cell survival during the unfolded protein response. *Mol Cell* 5: 897 – 904

Hetz C, Zhang K, Kaufman RJ (2020) Mechanisms, regulation and functions of the unfolded protein response. *Nat Rev Mol Cell Biol* 21: 421 – 438

Igea A, Mendez R (2010) Meiosis requires a translational positive loop where CPEB1 ensues its replacement by CPEB4. *EMBO J* 29: 2182 – 2193

Ivshina M, Lasko P, Richter JD (2014) Cytoplasmic polyadenylation element binding proteins in development, health, and disease. *Annu Rev Cell Dev Biol* 30: 393 – 415

Kamimura D, Bevan MJ (2008) Endoplasmic reticulum stress regulator XBP-1 contributes to effector CD8^{+} T cell differentiation during acute infection. *J Immunol* 181: 5433 – 5441

Keestra-Gounder AM, Byndloss MX, Seyffert N, Young BM, Chavez-Arroyo A, Tsai AY, Cevallos SA, Winter MG, Pham OH, Tiffany CR *et al* (2016) NOD1 and NOD2 signalling links ER stress with inflammation. *Nature* 532: 394 – 397

Kuleshov MV, Jones MR, Rouillard AD, Fernandez NF, Duan Q, Wang Z, Koplev S, Jenkins SL, Jagodnik KM, Lachmann A *et al* (2016) Enrichr: a comprehensive gene set enrichment analysis web server 2016 update. *Nucleic Acids Res* 44: W90 – W97

Langmead B, Salzberg SL (2012) Fast gapped-read alignment with bowtie 2. *Nat Methods* 9: 357 – 359

Langmead B, Trapnell C, Pop M, Salzberg SL (2009) Ultrafast and memory-efficient alignment of short DNA sequences to the human genome. *Genome Biol* 10: R25

Lee PP, Fitzpatrick DR, Beard C, Jessup HK, Lehar S, Makar KW, Perez-Melgosa M, Sweetser MT, Schlissel MS, Nguyen S *et al* (2001) A critical role for Dnmt1 and DNA methylation in T cell development, function, and survival. *Immunity* 15: 763 – 774

Leone RD, Zhao L, Englert JM, Sun IM, Oh MH, Sun IH, Arwood ML, Bettencourt IA, Patel CH, Wen J *et al* (2019) Glutamine blockade induces divergent metabolic programs to overcome tumor immune evasion. *Science* 366: 1013 – 1021

Liao Y, Smyth GK, Shi W (2019) The R package Rsubread is easier, faster, cheaper and better for alignment and quantification of RNA sequencing reads. *Nucleic Acids Res* 47: e47

Liberzon A, Birger C, Thorvaldsdottir H, Ghandi M, Mesirov JP, Tamayo P (2015) The molecular signatures database (MSigDB) hallmark gene set collection. *Cell Syst* 1: 417 – 425

Love MI, Huber W, Anders S (2014) Moderated estimation of fold change and dispersion for RNA-seq data with DESeq2. *Genome Biol* 15: 550

Ma X, Bi E, Lu Y, Su P, Huang C, Liu L, Wang Q, Yang M, Kalady MF, Qian J *et al* (2019) Cholesterol induces CD8(+) T cell exhaustion in the tumor microenvironment. *Cell Metab* 30: 143–156

Maillo C, Martin J, Sebastian D, Hernandez-Alvarez M, Garcia-Rocha M, Reina O, Zorzano A, Fernandez M, Mendez R (2017) Circadian- and UPR-dependent control of CPEB4 mediates a translational response to counteract hepatic steatosis under ER stress. *Nat Cell Biol* 19: 94–105

Ortiz-Zapater E, Pineda D, Martinez-Bosch N, Fernandez-Miranda G, Iglesias M, Alameda F, Moreno M, Eliscovich C, Eyras E, Real FX *et al* (2011) Key contribution of CPEB4-mediated translational control to cancer progression. *Nat Med* 18: 83–90

Perez-Guijarro E, Karras P, Cifdaloz M, Martinez-Herranz R, Canon E, Grana O, Horcajada-Reales C, Alonso-Curbelo D, Calvo TG, Gomez-Lopez G *et al* (2016) Lineage-specific roles of the cytoplasmic polyadenylation factor CPEB4 in the regulation of melanoma drivers. *Nat Commun* 7: 13418

Pique M, Lopez JM, Foissac S, Guigo R, Mendez R (2008) A combinatorial code for CPE-mediated translational control. *Cell* 132: 434–448

Quail DF, Joyce JA (2013) Microenvironmental regulation of tumor progression and metastasis. *Nat Med* 19: 1423–1437

Robichaud N, Hsu BE, Istomine R, Alvarez F, Blagih J, Ma EH, Morales SV, Dai DL, Li G, Souleimanova M *et al* (2018) Translational control in the tumor microenvironment promotes lung metastasis: phosphorylation of eIF4E in neutrophils. *Proc Natl Acad Sci U S A* 115: E2202–E2209

Sancho D, Mourao-Sa D, Joffre OP, Schulz O, Rogers NC, Pennington DJ, Carlyle JR, Reis e Sousa C (2008) Tumor therapy in mice via antigen targeting to a novel, DC-restricted C-type lectin. *J Clin Invest* 118: 2098–2110

Scheu S, Stetson DB, Reinhardt RL, Leber JH, Mohrs M, Locksley RM (2006) Activation of the integrated stress response during T helper cell differentiation. *Nat Immunol* 7: 644–651

Song M, Sandoval TA, Chae CS, Chopra S, Tan C, Rutkowski MR, Raundhal M, Chaurio RA, Payne KK, Konrad C *et al* (2018) IRE1alpha-XBP1 controls T cell function in ovarian cancer by regulating mitochondrial activity. *Nature* 562: 423–428

Tauriello DVF, Palomo-Ponce S, Stork D, Berenguer-Llergo A, Badia-Ramentol J, Iglesias M, Sevillano M, Ibiza S, Canellas A, Hernando-Momblona X *et al* (2018) TGFbeta drives immune evasion in genetically reconstituted colon cancer metastasis. *Nature* 554: 538–543

Thaxton JE, Wallace C, Riesenberg B, Zhang Y, Paulos CM, Beeson CC, Liu B, Li Z (2017) Modulation of endoplasmic reticulum stress controls CD4 (+) T-cell activation and antitumor function. *Cancer Immunol Res* 5: 666–675

Thorvaldsdottir H, Robinson JT, Mesirov JP (2013) Integrative genomics viewer (IGV): high-performance genomics data visualization and exploration. *Brief Bioinform* 14: 178–192

Tsai LY, Chang YW, Lee MC, Chang YC, Hwang PI, Huang YS, Cheng CF (2016) Biphasic and stage-associated expression of CPEB4 in hepatocellular carcinoma. *PLoS One* 11: e0155025

Villanueva E, Navarro P, Rovira-Rigau M, Sibilio A, Mendez R, Fillat C (2017) Translational reprogramming in tumour cells can generate oncoselectivity in viral therapies. *Nat Commun* 8: 14833

Wang M, Kaufman RJ (2014) The impact of the endoplasmic reticulum protein-folding environment on cancer development. *Nat Rev Cancer* 14: 581–597

Wek RC, Jiang HY, Anthony TG (2006) Coping with stress: eIF2 kinases and translational control. *Biochem Soc Trans* 34: 7–11

Wu D, Lim E, Vaillant F, Asselin-Labat ML, Visvader JE, Smyth GK (2010) ROAST: rotation gene set tests for complex microarray experiments. *Bioinformatics* 26: 2176–2182

Xu Y, Ruggero D (2020) The role of translation control in tumorigenesis and its therapeutic implications. *Annu Rev Cancer Biol* 4: 437–457

Yang X, Xia R, Yue C, Zhai W, Du W, Yang Q, Cao H, Chen X, Obando D, Zhu Y *et al* (2018) ATF4 regulates CD4(+) T cell immune responses through metabolic reprogramming. *Cell Rep* 23: 1754–1766